IOP Publishing Physics in Medicine and Biology

Phys. Med. Biol. **57** (2012) 6309–6326 doi:10.1088/0031-9155/57/20/6309

Dose conversion coefficients for paediatric CT examinations with automatic tube current modulation

H Schlattl, M Zankl, J Becker and C Hoeschen

Helmholtz Zentrum München—National Research Center for Environmental Health
Research Unit Medical Radiation Physics and Diagnostics, Ingolstädter Landstr. 1,
D-85764 Oberschleißheim, Germany

E-mail: helmut.schlattl@helmholtz-muenchen.de

Received 11 April 2012, in final form 8 August 2012
Published 19 September 2012
Online at stacks.iop.org/PMB/57/6309

Abstract

A common dose-saving technique used in modern CT devices is automatic tube current modulation (TCM), which was originally designed to also reduce the dose in paediatric CT patients. In order to be able to deduce detailed organ doses of paediatric models, dose conversion coefficients normalized to $CTDI_{vol}$ for an eight-week-old baby and seven- and eight-year-old children have been computed accounting for TCM. The relative difference in organ dose conversion coefficients with and without TCM is for many organs and examinations less than 10%, but can in some cases amount up to 30%, e.g., for the thyroid in the chest CT of the seven-year-old child. Overall, the impact of TCM on the conversion coefficients increases with increasing age. Besides TCM, also the effect of collimation and tube voltage on organ dose conversion coefficients has been investigated. It could be shown that the normalization to $CTDI_{vol}$ leads to conversion coefficients that can in most cases be considered to be independent of collimation and tube voltage.

(Some figures may appear in colour only in the online journal)

1. Introduction

Computed tomography (CT) is one of the most valuable imaging modalities in medicine. The rapid development in CT technology, in particular, the shorter scan times due to faster gantry rotations and the usage of multi-slice detectors, opened the path for new applications. Certainly, an increasing usage of CT in emergency departments could be observed (Broder *et al* 2007), which appears to be one of the major reasons for higher number of CT scans in paediatrics. The proportions of paediatric CT examinations vary from 1% in Germany (Galanski *et al* 2006), 3% in Japan (Chodick *et al* 2006), 6% in USA (CRCPD 2007) and 11% in the UK (Mettler *et al* 2000). While these fractions seem to be in most cases rather low, the higher sensitivity of children to ionizing radiation and longer expected lifetime must

be considered. According to the Committee on the Biological Effects of Ionizing Radiations (BEIR 1980) or the International Commission on Radiological Protection (ICRP 2007), the lifetime attributable cancer mortality risk is at least twice as high for children under 10 than for a 30–40-year-old adult.

Until the beginning of this millennium, most manufacturers did not supply special protocols for paediatric CT examinations, such that often the settings for adults were used in the clinics (Paterson *et al* 2001). Since the body diameter of children, particularly before adolescence, is considerably lower than that of adults, this certainly led to unnecessarily high radiation exposure. In 2001, this problem was brought to widespread attention by a series of publications (Rogers 2001, Paterson *et al* 2001, Brenner *et al* 2001, Donnelly *et al* 2001) about CT in paediatrics. In the following years, the CT manufacturers introduced special scanning protocols for children, and new dose-saving techniques (Fox and Toth 2002, Suess and Chen 2002, Westerman 2002).

The main dose-saving technique is certainly the automatic tube current modulation (TCM), which is also applied in adult CT scans. It accounts for the varying attenuation of the human body along the body axis ('longitudinal') and in the transverse plane ('angular'). All main CT manufacturers implemented attenuation-based TCM under different notations (GE: Smart mA, Philips: Z-DOM, Siemens: CareDose 4D^{TM}, Toshiba: ^{Sure}Exposure, see McCollough *et al* (2006)). In a previous work (Schlattl *et al* 2010, paper I), the implementation of an attenuation-based TCM in a Monte Carlo transport code (EGSnrc, Kawrakow *et al* 2010) has been described in detail.

For reliable estimates of patient organ doses or effective doses (ICRP 2007) in general, measurable dose quantities like air kerma free in air or $CTDI_{vol}$ are to be related to the organ doses. For this purpose, dose conversion coefficients are computed with the help of particle transport Monte Carlo codes. These require anatomically correct models of the patient. First dose estimates for infants in CT (Huda *et al* 1997) were obtained by scaling the results from adults appropriately (Atherton and Huda 1996). Alternative estimates are based on the conversion coefficients computed by Khursheed *et al* (2002), where models for children of various ages are employed (Cristy and Eckerman 1987). In all these cases, MIRD-type (Snyder *et al* 1969) models have been used that consist of simple geometric shapes for the organs. The first paediatric models based on tomographic data were created by Veit *et al* (1989). The models are based on CT data sets of an eight-week-old baby and seven-year-old child. Resulting dose conversion coefficients for CT examinations (Zankl *et al* 1993) are still used in the CT dosimetry tool CT-Expo (Stamm and Nagel 2002).

In this work, updated versions of the models for an eight-week-old baby and seven-year-old child are employed. Additionally, a voxel model based on CT data of an eight-year-old girl has been developed. Dose conversion coefficients for 5 mm thick axial slices covering each body completely are computed with and without automatic TCM. By combining the results for each slice appropriately, organ dose conversion coefficients for basically all CT examinations can be deduced. In paper I, it has been shown that by this method, accurate conversion coefficients can also be obtained for spiral scans. However, since the largest collimation used was 5 mm, for this work dose conversion coefficients for spiral trajectories with collimations of up to 8 cm have been computed for the seven-year-old child, too, and compared with those from axial scans. Moreover, for this model, calculations for tube voltages of 80, 120 and 140 kV have been performed to demonstrate the influence of the tube voltage on the dose conversion coefficients. For the other models, the tube voltage was fixed to 120 kV.

Table 1. Selected properties of employed paediatric voxel models.

Model	Age	Body height (cm)	Weight (kg)	Voxel dimensions (mm^3)
Baby	Eight weeks	57	4.2	$0.85 \times 0.85 \times 4$
Child	Seven years	115	21.7	$1.54 \times 1.54 \times 8$
Jo	Eight years	130	34	$1.875 \times 1.875 \times 10$

2. Materials and methods

2.1. Voxel models

Baby and Child—phantoms of an eight-week-old baby and a seven-year-old child—were the first voxel phantoms constructed in our research group at the Helmholtz Zentrum München, German Research Center for Environmental Health (formerly: GSF—National Research Center for Environment and Health) (Petoussi-Henss *et al* 2002, Veit *et al* 1989, Zankl *et al* 1988, Zankl 2010). Jo is the phantom of an eight-year-old child that has been segmented recently by one of the authors (MZ). The Baby was constructed from computed tomographic image data of a dead body, Child and Jo from those of living female patients. For the creation of hermaphrodite models, testes have been added. Child is relatively small with a height and weight of 115 cm and 21.7 kg, respectively, and thus can serve as a model for a five-year-old reference child (ICRP 2002: 109 cm, 19 kg). Despite Jo's age of eight years, her dimensions of 130 cm and 34 kg closely resemble those of a ten-year-old reference child (ICRP 2002: 138 cm, 32 kg).

The data sets consist of large numbers of contiguous axial slices, where each slice is a matrix of 256×256 pixels (picture elements, in a planar image). The voxels (volume elements) are the pixels multiplied by the thickness of the slice. The single slice images are stacked, resulting in a three-dimensional array of voxels. The height of the voxel array, and thus the possible CT scan range, does not necessarily agree with the body height, as head, legs and feet might be inclined, bent or outstretched.

In the primary image data, each pixel has a value called 'Hounsfield number' or 'CT number' that is characteristic of the attenuation of x-rays of a specific radiation quality and visualized as a shade of grey. Thus, the image property coded by the 'grey value' is related to the tissue electron density, not to the anatomical site. Therefore, the anatomical boundaries between organs and tissues have to be determined on the basis of the grey values and grey value contrasts, and then each pixel is assigned to an organ or tissue to which the corresponding voxel belongs. This process of assigning each voxel to a specific organ is called segmentation and requires a certain amount of anatomical knowledge of the user. The segmentation procedures applied mainly were region growing, the use of thresholds and morphological operations, and manual drawing of organ boundaries. A rendered three-dimensional representation of the resulting models and some selected properties are provided in figure 1 and table 1, respectively.

The number and type of organs that were segmented in the individual voxel phantoms evolved in the course of time, and therefore the list of organ identification numbers is also different among the phantoms, depending on when they were segmented. The original versions of Baby and Child had 54 and 64 segmented objects, respectively. Meanwhile, Baby and Child were complemented with several objects, and the resulting revised versions have now 67 and 125 segmented organs and tissues, respectively. A list of organs missing in Baby and Child, but required to compute the effective dose as defined in ICRP (2007), together with the

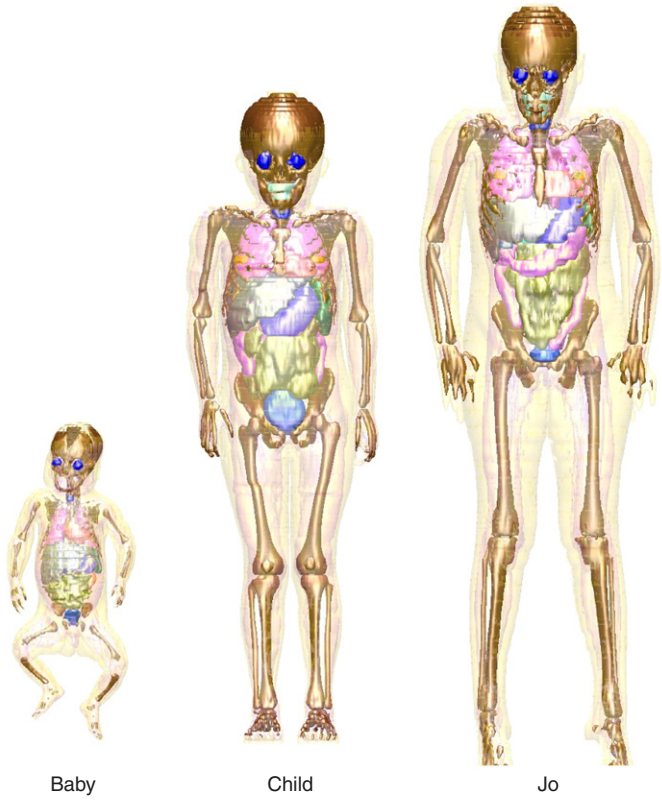

Figure 1. Images of presented models where breast, bones, colon, eyes, lungs, liver, pancreas, small intestine, stomach, teeth, thyroid and urinary bladder can be identified by different surface colours. Muscle and adipose tissues are made transparent. For illustration purposes, the voxelized surfaces have been smoothed.

Table 2. List of surrogate organs used in the respective model (column 3) to compute effective DCC^{CT} according to ICRP (2007).

Organ	Surrogate organ	Model
Breast	Glandular breast tissue	Baby
Endosteum	Spongiosa	Child, Jo
	Skeleton	Baby
Salivary glands	Thyroid	Baby
Extrathoracic airw.	Thyroid	Baby
Heart wall	Total heart	Baby
Lymphatic nodes	Residual tissue	Baby, Child
Oral mucosa	Thyroid	Baby

corresponding surrogate organs is provided in table 2. Jo has been equipped with all organs that have been defined in the adult reference computational phantoms of ICRP and ICRU (ICRP 2009), thus having a total of 136 individually segmented organs or tissues. Note that all models have been employed in the computations as illustrated in figure 1, i.e. including their arms.

2.2. Monte Carlo code

All computations have been performed employing the Monte Carlo particle transport code EGSnrc in version V4-2-3-0 (Kawrakow *et al* 2010). The physics and particle transport scheme conform with those of version V4-2-2-5 used in paper I. Like in that work, the CT scan is simulated with two different user codes that record either the number of photons in the central part of the detector to determine the TCM, or score the energy deposited in each organ to deduce organ dose conversion coefficients. In the first case, the path of photons (electrons) is followed until their energy falls below 10 keV (60 keV), while in the second code, the lower cut-off energy is 2 keV (20 keV). The remaining kinetic particle energy is deposited locally.

2.3. CT scan parameters

A Siemens SOMATOM Sensation Cardiac 16 device (Siemens Medical Solutions, Forchheim, Germany) with focus-to-isocentre and detector-to-isocentre distances of 57 and 43.5 cm, respectively, is modelled in the simulation[1]. The x-ray spectra have been determined using the spectrum generator SpekCalc (Poludniowski *et al* 2009), which is based on theoretical bremsstrahlung cross sections. A very good agreement with measurements is achieved by this method (Poludniowski 2007). In comparison with the spectrum generator by Cranley *et al* (1997), which is based on semi-empirical models and is used in paper I, the SpekCalc spectra are somewhat softer, but no impact is expected for the organ dose conversion coefficients.

Series of axial scans with total collimation $h_{\mathrm{col}} = 5$ mm covering the entire models have been simulated. For Child, conversion coefficients with tube voltages of 80, 120 and 140 kV have been computed, while for Baby and Jo, the tube potential was fixed to 120 kV. For all cases, CT examinations with and without automatic TCM have been modelled. An attenuation-based approach for TCM has been assumed, where the modulation of the current is indirectly proportional to the square root of the photon counts in the central part of the detector (cf paper I). The photon counts have been determined for all models and tube voltages in an extra simulation (see section 2.2).

As demonstrated in paper I, dose conversion coefficients for examinations of a certain body region can be obtained by combining the conversion coefficients of those axial slices covering this region. Nevertheless, only total collimations of up to 5 mm were investigated in that work. Therefore, as an exemplary case, spiral chest CTs of Child have been simulated, too, for typical collimations of a 4-, 64- and 128-slice CT, i.e. for $h_{\mathrm{col}} = 0.4$, 3.84 and 8 cm, a pitch (Ψ) of 1.4 and a tube potential of 120 kV. As usual, the pitch is defined as the table feed per rotation relative to the total collimation.

2.4. Weighted CTDI

Besides the human models, two voxel models representing the CTDI body and head phantom of 32 and 16 cm in diameter, respectively, have been employed to determine weighted-CTDI-to-air-kerma conversion coefficients. Both phantoms have a height of 15 cm and consist of perspex with a density of 1.10 g cm^{-3}. The in-plane resolution is 0.5×0.5 mm^2. Each phantom contains four holes at the edge and one hole in the centre of about 1 cm in diameter, which would accommodate pencil ionization chambers in a real setup. The holes have a height of 10 cm and are covered with 2.5 cm of perspex. In the simulation, these holes are assumed to

[1] Details of filter material and shape are the property of the manufacturer and cannot be disclosed.

be filled with air, and the respective air doses are determined. The weighted CTDI ($\mathrm{CTDI_w}$) is then given by

$$\mathrm{CTDI_w} = \tfrac{1}{3}\mathrm{CTDI}_{100,c} + \tfrac{2}{3}\mathrm{CTDI}_{100,p}, \tag{1}$$

where $\mathrm{CTDI}_{100,c}$ and $\mathrm{CTDI}_{100,p}$ are the mean air doses in the central and peripheral holes, respectively, integrated over a length of 100 mm. For each tube potential and CTDI phantom, 2×10^9 photon histories were followed. To demonstrate the impact of the collimation, h_{col} was varied from 0.5 to 16 cm.

2.5. Dosimetry

Mean organ dose conversion coefficients were computed with the help of the Monte Carlo transport code. In the axial scans, the histories of 40 million source photons were pursued in each slice. In each spiral scan, 100 million photon histories were followed. Organ absorbed doses and air kerma at the rotation axis (K_{a}) were recorded. The consequent coefficients of variance of the conversion coefficients are always less than 0.5% for the relevant organs within the respective fields of view; for many organs, they are considerably lower.

In both cases, the resultant organ dose conversion coefficients are normalized to air kerma at the rotation axis (DCC^K). Still, in order to determine the dose conversion coefficients for the examination of a specific body part from the axial-slice computations, the simulated organ doses in the slices within the scan range are to be summed and then related to the corresponding total air kerma. The slices at the edges usually contribute partly to the total dose (see paper I for more details). For the axial as well as spiral scans, the organ dose conversion coefficients per air kerma are converted into organ doses per $\mathrm{CTDI_{vol}}$ ($\mathrm{DCC}^{\mathrm{CT}}$) by

$$\mathrm{DCC}^{\mathrm{CT}} = \mathrm{DCC}^K \left(\frac{\mathrm{CTDI_w}}{K_{\mathrm{a}}}\right)^{-1} N_{\mathrm{R}}\,\Psi, \tag{2}$$

where $\mathrm{CTDI_w}/K_{\mathrm{a}}$ is the $\mathrm{CTDI_w}$ to the air-kerma conversion coefficient for the head or body CTDI phantom at the corresponding tube voltage. For the number of rotations N_{R} times the pitch Ψ, the general relation

$$N_{\mathrm{R}}\,\Psi = \frac{z_u - z_l}{h_{\mathrm{col}}} \tag{3}$$

holds, where z_u and z_l are the upper and lower boundaries of the scan region, respectively. Note that for a fixed tube current and examination, i.e. $z_u - z_l = \mathrm{const}$, the doses for organs completely within the scan region are in first order proportional to Ψ^{-1}, while air kerma at the axis is only proportional to N_{R}. Thus, for these organs, DCC^K is nearly inversely proportional to $N_{\mathrm{R}}\,\Psi$ and only a small dependence of $\mathrm{DCC}^{\mathrm{CT}}$ on collimation and pitch settings of an examination can be expected.

An overview of the main quantities and abbreviations used in this work and the analogue notation used by the International Atomic Energy Agency (IAEA 2007) is provided in table 3. The scan ranges for the most abundant paediatric CT examinations are provided in table 4 for the three phantoms of this work. Organ and effective dose conversion coefficients are presented for these examinations.

In all models, endosteum and red bone marrow (RBM) are not segmented explicitly, since the voxel dimensions are too large to resolve the fine structure of bone spongiosa. To determine the dose to RBM, the so-called three-factor formalism (Kramer 1982) is employed. It accounts for the different mass energy-absorption coefficient μ_{en}/ρ of RBM and the bone spongiosa, and for additional secondary electrons released in the bone trabeculae, but being stopped in RBM, using the enhancement factors of King and Spiers (1985). A detailed description is provided in paper I.

Table 3. List of abbreviations used in this work and the corresponding notation according to IAEA (2007).

	Notation	
Quantity	This work	IAEA (2007)
Incident air kerma	K_a	K_i
Pitch	Ψ	p
Slice thickness	h_{col}	NT
Number of rotations	N_R	–
Central CTDI	$CTDI_{100,c}$	$C_{PMMA,100,c}$
Peripheral CTDI	$CTDI_{100,p}$	$C_{PMMA,100,p}$
Weighted CTDI	$CTDI_w$	C_W
Volume CTDI	$CTDI_{vol}$	C_{VOL}
Dose conversion coefficient of tissue T		
...relative to kerma at axis	Tissue DCC^K	c_{D_T,K_i}
...relative to $CTDI_{vol}$	Tissue DCC^{CT}	$c_{D_T,C_{VOL}}$

Table 4. Start position (z_u) and scan range ($\Delta z = z_u - z_l$) for different CT examinations of the presented phantoms in centimetres. The start position is measured relative to the lower phantom boundary, which is usually the inferior surface of the bottommost toe. The parameters are determined by using the landmarks specified in a German CT survey (Brix *et al* 2003).

	Baby		Child		Jo	
	z_u	Δz	z_u	Δz	z_u	Δz
Brain	56.8	9.2	116.0	13.6	136.0	14.0
Face/sinuses	52.0	6.0	108.0	8.8	127.0	10.0
Chest	42.8	9.6	95.2	14.4	115.0	17.0
Abdomen/pelvis	35.6	17.2	84.8	31.2	104.0	34.0
Lumbar spine	32.0	8.4	76.8	13.6	94.0	17.0

Since for endosteum, neither the elemental composition, nor the mass in the individual bones, nor enhancement factors are available, the three-factor method is not applicable there. Hence, the mean dose to bone spongiosa is used as a substitute.

3. Results and discussion

3.1. CTDI$_w$

The conversion coefficients $CTDI_w/K_a$ relating the weighted CTDI to air kerma at the rotation axis are summarized in table 5. For $h_{col} \leqslant 5$ cm, the relative differences in $CTDI_w/K_a$ are below 1%, i.e. considerably below the $1\,\sigma$ statistical uncertainty of about 3%. These results are in agreement with the findings of Li *et al* (2011), who found no significant difference in the $CTDI_w$ values for collimations up to 4 cm. Moreover, they could confirm good agreement between measurements and Monte Carlo simulations, such that it is justified to assume that also for larger collimations, the results from the Monte Carlo simulations are reliable.

Since no significant difference in $CTDI_w$ is observed for collimations up to 5 cm, the average value at $h_{col} = 0.5$, 2 and 5 cm is used in the following for each voltage and phantom. At $h_{col} = 10$ cm, $CTDI_w$ is at most about 6% lower compared to the case $h_{col} \leqslant 5$ cm. Taking into account other uncertainties in the calculations (photon cross sections, finite x-ray focal spot size, exact x-ray filtering, etc), this error is still considered to be negligible, and thus a single value for $CTDI_w/K_a$ for $h_{col} \leqslant 10$ cm is applicable. For larger collimations, like for

Table 5. Ratios of $CTDI_w$ to air kerma on the rotation axis (K_a) for different voltages and collimations (h_{col}) using CTDI body and head phantoms and the filtration described in section 2.3. The first row for each voltage provides the mean of $CTDI_w/K_a$ at 0.5, 2 and 5 cm. The relative differences to those mean values are provided in the columns denoted by '%'.

Tube voltage (kV)	h_{col} (cm)	Body $CTDI_w/K_a$ (mGy/mGy)	Body (%)	Head $CTDI_w/K_a$ (mGy/mGy)	Head (%)
80		0.209		0.471	
	0.5	0.210	1	0.474	1
	2.0	0.209	0	0.472	0
	5.0	0.208	−1	0.468	−1
	10.0	0.202	−3	0.445	−6
	16.0	0.165	−21	0.327	−31
120		0.257		0.544	
	0.5	0.255	−1	0.546	0
	2.0	0.261	1	0.545	0
	5.0	0.255	−1	0.541	−1
	10.0	0.248	−4	0.516	−5
	16.0	0.201	−22	0.378	−31
140		0.268		0.567	
	0.5	0.271	1	0.565	0
	2.0	0.267	−1	0.567	0
	5.0	0.267	0	0.568	0
	10.0	0.257	−4	0.531	−6
	16.0	0.209	−22	0.390	−31

$h_{col} = 16$ cm, not all primary radiation can be recorded by the 10 cm long dosimeters leading, as expected, to a significant decrease in $CTDI_w/K_a$.

For comparison, the values for $h_{col} = 5$ mm using the spectrum generator by Cranley *et al* (1997) are 0.260 and 0.552 mGy/mGy for the CTDI body and head phantom, respectively, at 120 kV. Thus, the influence of the employed spectrum generator on the $CTDI_{vol}$-per-air-kerma values is at most about 2% and it is not expected that the effect is higher for the organ dose conversion coefficients.

3.2. Dependence of DCC^{CT} on collimation

As demonstrated in paper I for adult models, the dose conversion coefficients for any CT examination can be determined reliably by combining the conversion coefficients from a series of axial slices. Nevertheless, the largest collimation used then was 0.5 cm. Therefore, as an example, spiral chest CT examinations of Child have been simulated using collimations of 0.4, 3.84 and 8 cm at 120 kV with $\Psi = 1.4$ with and without TCM.

In figure 2(b), the organ DCC^{CT} by combining axial slices using (2) with $N_R\,\Psi = 1$ (thus, $CTDI_{vol} = CTDI_w$) are shown for the most relevant organs at constant tube current. The relative differences of DCC^{CT} from the spiral scans to those from the axial scan are presented in figure 2(a). As in paper I, for $h_{col} = 0.4$ mm, the organ DCC^{CT} of axial and spiral scans are very similar. For $h_{col} = 3.84$ and 8 cm, the organ DCC^{CT} differ by at most 10 and about 80%, respectively, from DCC^{CT} of the axial scans. However, for collimations of a few centimetres or higher, it is important to know the initial direction of the spiral trajectory (see also Zhang *et al* (2009)), i.e. whether the tube was irradiating the patient in the beginning, e.g., in the antero-posterior (a.p.) or postero-anterior (p.a.) direction, abbreviated as 'a.p. spiral' and 'p.a.

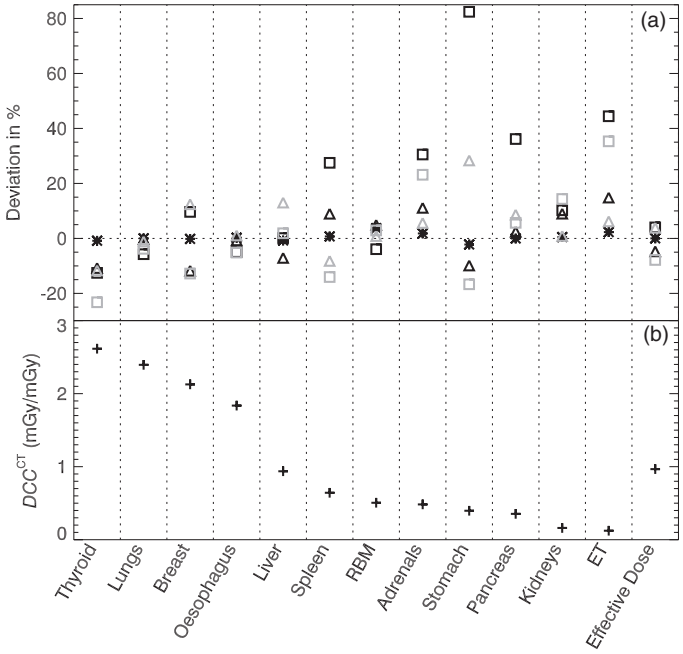

Figure 2. (a) Comparison of conversion coefficients for chest CT of Child at 120 kV without TCM in axial or spiral mode and different collimations. (b) DCC^{CT} of the most relevant organs combining axial slices with $h_{col} = 5$ mm are shown. In (a) the relative difference to these conversion coefficients from spiral trajectories with $h_{col} = 0.4$ (∗), 3.84 (△) and 8 cm (□) and $\Psi = 1.4$ is given. Trajectories starting in the a.p. direction are in bold, while those beginning in the opposite direction are in light grey. Since the coefficients of variance are well below 0.5% (see section 2.5), error bars are omitted.

spiral', respectively, in the following. Thus, in addition to the a.p. spirals computed usually, p.a. spirals have been simulated, too. For most organs within the scan region, like liver or breast, it is observed that the change from an a.p. to a p.a. spiral leads to about the same relative difference in organ DCC^{CT} compared to the axial case, but with an opposite sign. Thus, to obtain more accurate organ DCC^{CT} at larger collimations by not combining axial scans, but following the proper spiral trajectories, it is essential to know the exact start position of the x-ray tube. This finding is in agreement with Zhang *et al* (2009), who have shown, in addition, that also the pitch of the spiral is an important parameter for larger collimations. For small collimations, DCC^{CT} from axial scans provide for most relevant organs reliable DCC^{CT} even for collimations up to 8 cm. Exceptions are organs at the edge of the scan field like, for chest CT, stomach, ET, pancreas and adrenals, DCC^{CT} of which are, however, usually small compared to the organs fully within the scan range. Thus an error of 80% in the worst case but generally not higher than 40% might still be acceptable for organs at the scan edge.

A special case is the thyroid, which is at the beginning of the scan range and is completely inside the scan range, thus having a large DCC^{CT}. In Child, the thyroid is partly shielded by the chin, the shoulders and the spine, such that the highest contribution to DCC^{CT} comes from oblique directions. In axial scans the thyroid is exposed from all four possible oblique directions, i.e. left or right, anterior or posterior oblique source positions. But for all spiral trajectories with $h_{col} \geqslant 3.84$ cm, the thyroid is exposed predominantly only from one oblique direction, as its cranio-caudal extent is small. Thus, the thyroid DCC^{CT} for the spirals with

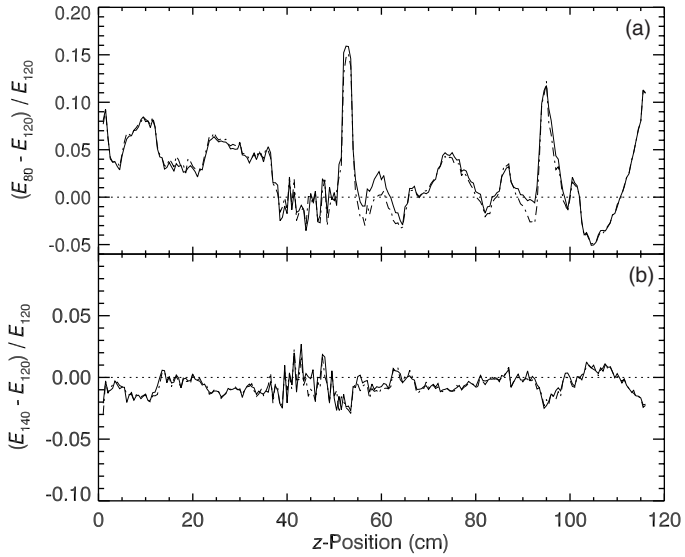

Figure 3. Relative difference of the effective DCC^{CT} (E) at 80 (a) and 140 kV (b) to the effective DCC^{CT} at 120 kV for different slice positions in Child with (dash-dotted line) or without TCM (solid).

$h_{col} \geqslant 3.84$ cm is always significantly smaller than that from the axial slices, but in most cases the difference is still below 15%.

The same spiral trajectories have been computed with TCM, too, and the resulting DCC^{CT} been compared with those from axial scans. While the organ DCC^{CT} might differ significantly (see also table 6), the relative differences between spiral and axial DCC^{CT} are very similar to those in figure 2(a).

It should be noted that all spirals start at the same height (see table 4) to quantify the uncertainty in determining DCC^{CT} from axial scans. In actual CT scans, a larger collimation leads to a more extended overscanning region, which would be accounted for in the computation of the conversion coefficients by extending the region over which axial slices are combined. Hence, it cannot be inferred from figure 2(b) how organ doses behave for different collimations. Moreover, accurate DCC^{CT} at the edge of the scanning region can only be obtained when the exact overscanning region is known, i.e. how many additional rotations are made and whether adaptive apertures are employed to minimize that radiation at the scan edges which cannot be used for reconstruction.

3.3. Dependence of DCC^{CT} on tube voltage

For Child, axial scans with tube voltages of 80, 120 and 140 kV have been simulated and for each axial slice, the effective DCC^{CT} has been deduced. In figure 3 the relative difference of the effective DCC^{CT} of 80 and 140 kV with respect to 120 kV has been shown for each slice position. Apart from a few exceptional z-positions, the relative differences are always below a few per cent. This demonstrates that the weighting of central-to-peripheral dose of $1/2$ in the definition of $CTDI_w$ (1) rather well reproduces the dependence of the effective dose on the tube potential. This has also been proven for the ICRP/ICRU reference male adult model (ICRP 2009) in a side computation. There, the relative differences of effective DCC^{CT} between 80

Table 6. List of organ DCC^{CT} in mGy/mGy and effective dose DCC^{CT} in mSv/mGy of Child for the CT examinations of table 4 with different voltages, with and without TCM. For the brain examination, the conversion coefficients are related to $CTDI_w^{head}$, while all others are normalized to $CTDI_w^{body}$. A list of surrogate organs used in the computation of the effective DCC^{CT} is provided in table 2. For DCC^{CT} of 80 and 140 kV the relative differences from those at 120 kV are provided, too ('%').

	Without TCM					With TCM				
Tube voltage (kV):	80		120	140		80		120	140	
Organ		(%)			(%)		(%)			(%)
					Brain					
Brain	1.21	−3	1.25	1.25	0	1.30	−4	1.36	1.35	0
Eyes	1.02	−1	1.04	1.03	−1	1.19	1	1.18	1.20	1
Extrath. airw.	0.43	−10	0.47	0.48	1	0.49	−8	0.53	0.55	3
Salivary glands	0.16	−12	0.18	0.18	1	0.18	−11	0.20	0.21	3
RBM	0.18	−5	0.19	0.19	−1	0.17	−5	0.18	0.18	0
Effect. dose	0.048	−7	0.052	0.052	0	0.050	−7	0.054	0.054	1
					Face/sinuses					
Eyes	2.41	5	2.29	2.27	−1	2.58	7	2.41	2.42	0
Extrath. airw.	2.05	−1	2.08	2.09	1	1.95	−1	1.97	1.99	1
Salivary glands	2.21	9	2.04	2.01	−1	1.91	7	1.78	1.76	−2
Brain	1.20	1	1.19	1.19	0	1.28	0	1.28	1.27	−1
Oral mucosa	0.93	−6	0.99	1.00	2	0.84	−5	0.88	0.91	3
RBM	0.26	−2	0.27	0.27	0	0.26	−1	0.27	0.27	0
Thyroid	0.23	−8	0.24	0.24	0	0.21	−8	0.22	0.22	0
Skin	0.17	8	0.16	0.15	−1	0.17	8	0.16	0.15	−1
Effect. dose	0.121	−2	0.123	0.123	0	0.115	−2	0.117	0.118	0
					Chest					
Thyroid	2.94	12	2.61	2.55	−2	1.95	8	1.80	1.73	−4
Heart	2.81	4	2.70	2.66	−1	2.73	4	2.64	2.61	−1
Lungs	2.46	3	2.39	2.38	0	2.24	1	2.21	2.19	−1
Breast	2.19	3	2.13	2.14	1	2.31	4	2.23	2.24	0
Oesophagus	1.82	−1	1.84	1.84	0	1.69	−3	1.73	1.73	0
Liver	0.94	1	0.94	0.93	0	1.07	1	1.06	1.06	0
Spleen	0.63	−2	0.64	0.64	0	0.72	−1	0.73	0.73	0
RBM	0.49	−4	0.51	0.51	1	0.44	−5	0.47	0.47	1
Stomach	0.39	−2	0.40	0.40	0	0.44	−2	0.45	0.45	0
Effect. dose	0.99	2	0.97	0.97	0	0.94	1	0.92	0.92	0
					Abdomen/pelvis					
Small intestine	3.14	5	3.00	2.96	−1	3.00	3	2.90	2.84	−2
Urinary bladder	3.09	5	2.95	2.93	0	2.62	2	2.57	2.52	−2
Stomach	3.05	5	2.90	2.84	−2	3.13	5	2.97	2.93	−1
Gonads	2.96	1	2.95	2.93	0	2.69	−1	2.72	2.69	−1
Colon	2.85	2	2.80	2.76	−1	2.69	2	2.64	2.62	−1
Kidneys	2.74	2	2.69	2.69	0	2.61	1	2.59	2.57	−1
Pancreas	2.68	−1	2.69	2.69	0	2.71	−1	2.74	2.72	−1
Liver	2.52	2	2.46	2.45	0	2.62	2	2.57	2.55	−1
Spleen	2.50	2	2.45	2.43	−1	2.67	3	2.59	2.57	−1
Adrenals	2.38	−2	2.44	2.45	0	2.39	−3	2.47	2.48	0
Effect. dose	1.59	2	1.57	1.56	−1	1.53	1	1.52	1.50	−1

Table 6. (Continued.)

	Without TCM				With TCM			
Tube voltage (kV):	80		120	140	80		120	140
Organ		(%)		(%)		(%)		(%)
				Lumbar spine				
Small intestine	2.59	6	2.45	2.41 −2	2.47	5	2.35	2.32 −1
Gonads	2.48	2	2.45	2.43 −1	2.28	1	2.25	2.24 0
Kidneys	2.24	3	2.17	2.16 −1	2.10	2	2.06	2.04 −1
Colon	2.17	4	2.09	2.07 −1	2.10	3	2.03	2.00 −1
Stomach	1.66	7	1.56	1.54 −1	1.66	6	1.57	1.54 −2
Pancreas	1.48	0	1.48	1.48 0	1.47	−0	1.47	1.47 0
Spleen	1.08	3	1.05	1.04 −1	1.14	4	1.10	1.09 −1
Liver	0.73	0	0.73	0.72 −1	0.76	1	0.75	0.75 −1
Adrenals	0.65	−5	0.69	0.69 0	0.64	−5	0.67	0.68 0
Urinary bladder	0.37	−7	0.39	0.39 0	0.35	−7	0.37	0.37 0
Effect. dose	0.77	2	0.75	0.75 0	0.75	2	0.74	0.73 −1

and 120 kV are somewhat larger than for Child, but still for all z-positions, below 12% (see also Schlattl *et al* (2012)).

The largest differences of 10–15% are observed between 80 and 120 kV for Child at $z \approx 52$ cm and $z \approx 95$ cm, where testes and thyroid, respectively, are located. Both organs are located rather off centre, and thus their dependence on the tube potential is only badly described by the central-to-peripheral dose weighting of $CTDI_w$.

For $z < 52$ cm only the legs are directly irradiated, and thus only the skin dose contributes to the effective dose. This leads to an effective DCC^{CT} for $z = 51.5$ cm of about 0.005 mSv/mGy for all tube voltages. For $z = 53$ cm, the effective DCC^{CT} is about seven times higher, since there the testes are fully within the x-ray field.

The relative differences of the effective DCC^{CT} between 140 and 120 kV is always less than 4%, reflecting the small difference in penetration depth for the 120 and 140 kV spectra. Notably, the relative differences are in all cases rather insensitive to whether TCM is used or not.

For all examinations of table 4, organ DCC^{CT} are computed using (2) for all three tube voltages with and without TCM. In table 6 a list of selected organ DCC^{CT} and of the corresponding effective DCC^{CT} is provided. The relative difference of effective DCC^{CT} of 80 and 140 kV with respect to 120 kV is smaller than for the individual slices. Only for a few organ DCC^{CT} are the relative differences higher than 10%, i.e. the salivary glands DCC^{CT} in the brain examination and the thyroid DCC^{CT} in the chest scan. As for the individual slices (figure 3), the relative DCC^{CT} differences between 140 and 120 kV are smaller than between 120 and 80 kV, and this behaviour is independent of whether TCM is used or not. Overall, the dependence of organ and effective DCC^{CT} on the tube potential is small.

3.4. Dependence of DCC^{CT} on model and TCM

For all three models, organ and effective DCC^{CT} have been computed with and without TCM, but fixed tube voltage of 120 kV. The same list of CT examinations has been used as before (table 4). The organ DCC^{CT} of Baby are usually 20–80% higher than for Child or Jo (table 7), reflecting the lower body diameter of Baby compared to Child and Jo. This translates into effective DCC^{CT} of Baby being about 30–50% higher than those for Child or Jo. For the brain CT examination, the effective DCC^{CT} of Baby is even a factor 2 higher than that of Child

Table 7. List of organ DCC^{CT} in mGy/mGy and effective dose DCC^{CT} in mSv/mGy for the CT examinations of table 4 without and with TCM. The relative change in DCC^{CT} when enabling TCM is provided for each model, too ('%'). For the brain examination, the conversion coefficients are related to $CTDI_w^{head}$, while all others are normalized to $CTDI_w^{body}$. Salivary glands, oral mucosa and extrathoracic airways are not segmented in Baby. A list of surrogate organs used in the computation of the effective DCC^{CT} is provided in table 2.

	Baby			Child			Jo		
				TCM					
Organ	off	on	(%)	off	on	(%)	off	on	(%)
				Brain					
Brain	1.67	1.70	2	1.25	1.36	8	1.21	1.33	11
Eyes	1.47	1.58	8	1.04	1.18	14	0.78	0.91	16
Extrath. airw.	–	–	–	0.47	0.53	12	0.44	0.50	15
Salivary glands	–	–	–	0.18	0.20	11	0.21	0.23	12
RBM	0.50	0.51	3	0.19	0.18	−2	0.18	0.18	−3
Effect. dose	0.105	0.108	4	0.052	0.054	4	0.049	0.052	5
				Face/sinuses					
Eyes	3.10	3.13	1	2.29	2.41	6	2.02	2.04	1
Extrath. airw.	–	–	–	2.08	1.97	−5	2.07	2.01	−3
Salivary glands	–	–	–	2.04	1.78	−13	2.11	1.94	−8
Brain	1.67	1.68	1	1.19	1.28	8	0.91	0.96	5
Oral mucosa	–	–	–	0.99	0.88	−11	1.57	1.52	−3
RBM	0.83	0.84	1	0.27	0.27	−1	0.24	0.24	0
Thyroid	0.33	0.32	−1	0.24	0.22	−8	0.45	0.43	−4
Skin	0.33	0.33	0	0.16	0.16	0	0.16	0.16	0
Effect. dose	0.188	0.189	1	0.123	0.117	−5	0.139	0.136	−3
				Chest					
Thyroid	1.55	1.43	−7	2.61	1.80	−31	2.00	1.37	−32
Heart	3.66	3.55	−3	2.70	2.64	−2	2.15	1.93	−10
Lungs	3.45	3.35	−3	2.39	2.21	−8	2.00	1.69	−16
Breast	3.28	3.30	1	2.13	2.23	5	1.87	1.80	−4
Oesophagus	2.85	2.81	−1	1.84	1.73	−6	1.80	1.41	−21
Liver	1.44	1.46	2	0.94	1.06	13	1.05	1.05	0
Spleen	0.94	0.97	3	0.64	0.73	14	0.83	0.84	2
RBM	0.78	0.76	−2	0.51	0.47	−8	0.45	0.40	−13
Stomach	0.58	0.59	2	0.40	0.45	13	0.86	0.88	3
Effect. dose	1.39	1.37	−1	0.97	0.92	−4	0.92	0.82	−11
				Abdomen/pelvis					
Small intestine	3.93	4.02	2	3.00	2.90	−3	2.57	2.34	−9
Urinary bladder	4.01	3.29	−18	2.95	2.57	−13	2.22	1.84	−17
Stomach	3.64	4.16	15	2.90	2.97	3	2.26	2.28	1
Gonads	3.76	3.22	−14	2.95	2.72	−8	2.21	1.90	−14
Colon	3.70	3.75	1	2.80	2.64	−5	2.47	2.31	−7
Kidneys	3.72	4.02	8	2.69	2.59	−4	2.30	2.16	−6
Pancreas	3.41	3.84	13	2.69	2.74	2	2.15	2.12	−2
Liver	3.47	3.91	13	2.46	2.57	4	2.05	2.07	1
Spleen	3.36	3.83	14	2.45	2.59	6	2.02	2.09	4
Adrenals	3.26	3.66	12	2.44	2.47	1	2.02	1.95	−3
Effect. dose	2.03	2.07	2	1.57	1.52	−3	1.34	1.26	−6

Table 7. (Continued.)

	Baby			Child			Jo		
				TCM					
Organ	off	on	(%)	off	on	(%)	off	on	(%)
				Lumbar spine					
Small intestine	3.51	3.39	−3	2.45	2.35	−4	2.10	1.95	−7
Gonads	1.12	1.00	−11	2.45	2.25	−8	1.17	1.05	−10
Kidneys	3.36	3.40	1	2.17	2.06	−5	1.54	1.44	−6
Colon	3.02	2.95	−2	2.09	2.03	−3	1.84	1.77	−4
Stomach	2.41	2.57	6	1.56	1.57	1	0.63	0.61	−3
Pancreas	2.91	3.06	5	1.48	1.47	−1	0.68	0.65	−3
Spleen	1.71	1.80	6	1.05	1.10	5	0.47	0.47	0
Liver	1.65	1.73	5	0.73	0.75	3	0.51	0.51	0
Adrenals	2.51	2.62	4	0.69	0.67	−2	0.59	0.57	−3
Urinary bladder	0.65	0.59	−9	0.39	0.37	−5	0.37	0.34	−7
Effect. dose	1.08	1.09	1	0.75	0.74	−2	0.54	0.52	−5

or Jo. A notable exception to this general behaviour is the thyroid in the chest CT, the DCC^{CT} of which is considerably smaller for Baby than for Child or Jo. A close inspection revealed that the portion of the thyroid within the scan range is smaller for Baby than for Child or Jo. Thus, the smaller thyroid DCC^{CT} of Baby is caused by its posture and the scan ranges used in this work, and it does not necessarily mean that the thyroid DCC^{CT} of a chest CT is always smaller for babies than for older children.

Besides, it should be considered that especially for Baby, a variety of surrogate organs have been used for the computation of the effective DCC^{CT}. To estimate the introduced uncertainty, 'surrogate' effective DCC^{CT} for Jo have been computed using the same surrogate organs as for Baby (table 2). For brain, face/sinuses and chest CT, they differ by about 5% from the actual effective dose (table 7), while for abdomen/pelvis and lumbar spine CT, the differences are at most 1%. The larger differences between 'surrogate' and actual effective DCC^{CT} for chest CT and above can be attributed to those head organs where the thyroid, which is close to but below the head, is used as surrogate. It can be expected that by these considerations, an upper limit to the effective DCC^{CT} uncertainty by using surrogate organs in Baby is given, because in Baby the distance between thyroid and head is smaller than in Jo.

The relative organ DCC^{CT} differences of Child and Jo are usually below about 30%. In a few cases, larger differences of up to a factor 2 are observed for organs at the edge of the scan range, like, e.g., thyroid DCC^{CT} for face/sinuses, stomach DCC^{CT} for chest, and gonads (ovaries) DCC^{CT} for lumbar spine CT, caused by different fractions of the organ being within the scan range. Overall, the difference in effective DCC^{CT} between Child and Jo tends to increase for lower body areas, such that for a lumbar spine CT, the effective DCC^{CT} is about 30% lower for Jo than for Child, while for a chest CT, the difference is at most about 10% (with TCM). This is plausible when regarding the stature of Child and Jo (figure 1): the diameter and length of the chest are rather similar, while the abdomen of Jo is longer and has a larger diameter yielding lower organ DCC^{CT} for Jo than for Child.

TCM can alter the organ DCC^{CT} considerably by more than 30%, as for the thyroid of Child and Jo in a chest CT. This finding is in agreement with paper I, where for adults also the thyroid DCC^{CT} showed the greatest sensitivity to TCM, especially in chest CT. Nevertheless, for Baby the biggest change in the organ DCC^{CT} can be observed not in the chest CT, but in an abdomen/pelvis CT. This can be explained by the different shape of the Baby's trunk and

lesser developed pelvis compared to that of Child or Jo (cf figure 1). Thus, the attenuation in the Baby's lower abdomen and pelvis region is smaller than in the upper abdomen, while in Jo and Child the attenuation is only weakly dependent on the body height in that area. Longitudinal TCM leads then in Baby to higher DCC^{CT} for organs in the upper abdomen such as stomach, liver and pancreas, and lower DCC^{CT} for urinary bladder and gonads. Notably, the lower DCC^{CT} of urinary bladder and gonads of Child and Jo when enabling TCM are caused predominantly by angular TCM. Angular TCM leads to a higher tube current, and thus higher exposure in the lateral direction—where these organs are rather well shielded by the pelvis—and hence a reduced exposure in the a.p. and p.a. direction.

While the difference between TCM enabled or disabled can be substantial for individual organ DCC^{CT}, the influence of TCM on the effective DCC^{CT} is in most cases weak. It can be observed, however, that with increasing age, the sensitivity of the effective DCC^{CT} on TCM increases, such that the relative difference in the effective DCC^{CT} of Jo with or without TCM reaches 11% for a chest CT. In paper I it has been shown that, for adult models, TCM leads to a reduction of the effective DCC^{CT} of 4–15% for the same examination depending on the stature of the patient. Thus, the effect of TCM on the effective DCC^{CT} of paediatric patients shortly before or during adolescence is very similar to that of adult patients.

3.5. General remarks

When applying the presented DCC^{CT} two aspects should be considered. Firstly, for a chest CT, the patients are asked to lift their arms, if possible. Test computations for Child with arms removed showed organ and effective DCC^{CT} of at most 7% and 4%, respectively, higher than those with arms. For collimations below 4 cm this difference should be considered, but for larger collimations it seems to be negligible as long as the exact spiral trajectory is not known (cf section 3.2).

Secondly, Turner *et al* (2010) have demonstrated for four different CT scanners that dose conversion coefficients normalized to $CTDI_{vol}$ depend only weakly on the specific CT scanner. In view of that finding and summarizing the results of this work for different collimations and tube voltages, it is for most cases sufficient to compute a single set of conversion coefficients (normalized to $CTDI_{vol}$) for all tube voltages and CT devices with up to 128 slices ($h_{col} \lesssim 8$ cm).

4. Conclusion

Dose conversion coefficients for CT examinations of three paediatric models of different ages have been computed with and without tube current modulation (TCM). With this work, the results for adult models (paper I) have been extended to younger patients. Moreover, some additional aspects have been addressed, which might have a larger influence on paediatric than on adult models: the impact of tube voltage and total collimation on the conversion coefficients.

Dose conversion coefficients normalized to $CTDI_{vol}$ are computed by combining the results of two simulations, which provide $CTDI_w$ and organ doses normalized to K_a, respectively. Therefore, first the dependence of $CTDI_w/K_a$ on collimations up to 16 cm has been examined using voxel models of CTDI head and body phantoms. In both cases, this ratio is nearly constant up to a collimation of 10 cm, and then decreases by about 31% and 22% for the head and body phantom, respectively, when increasing h_{col} to 16 cm, independent of the tube voltage. Since the relative change of $CTDI_w/K_a$ with h_{col} is insensitive to the tube voltage, we conclude that the relative change is independent of the x-ray spectrum and thus of the detailed filter material and shape used.

Using a constant $CTDI_w/K_a$ ratio, organ DCC^{CT} of spiral chest CT scans for collimations of 0.4, 3.84 and 8 cm have been deduced. Conversion coefficients of organs fully within the scan range show relative differences of up to 10%, while DCC^{CT} of organs at the scan edges can differ by up to 80% when changing the collimation. However, for large collimations the relative differences are strongly dependent on the exact x-ray irradiation direction at the start of the scan. Without that knowledge, the average DCC^{CT} of spiral trajectories with various starting positions have to be used, which then are for most organs much less depending on the collimation. It can be expected that for adult models, the sensitivity on the collimation is generally smaller, since the scan ranges are longer and thus organ DCC^{CT} are less influenced by the exact spiral trajectory. Hence, it appears still to be justified to use a single set of conversion coefficients for collimations of up to 8 cm, which is about the collimation of CT devices with 128 detector rows.

The impact of the tube voltage on organ DCC^{CT} has been deduced. It has been demonstrated that for Child, conversion coefficients normalized to $CTDI_{vol}$ are only weakly dependent on the tube voltage with and without TCM. The same results have been found for adult models (Schlattl *et al* 2012).

The impact of TCM on the organ DCC^{CT} is for some organs and examinations substantial. For instance, the thyroid DCC^{CT} of a chest CT and urinary bladder DCC^{CT} of an abdomen/pelvis CT are reduced by up to 30% and 17%, respectively, when TCM is enabled. Nonetheless, in many cases the relative difference in organ DCC^{CT} without and with TCM is less than 10%, particularly for the younger models Baby and Child. For these models, the relative difference in the effective DCC^{CT} is always less than 5%. For Jo, enabling TCM can reduce the effective DCC^{CT} by up to 11% (for the chest CT), and thus the impact of TCM becomes comparable to that of an adult (paper I). However, it cannot be concluded what the net effect of TCM on the effective dose is. It is worth noting that in clinical practice $CTDI_{vol}$ is on average larger in examinations with than without TCM (Galanski *et al* 2006), and thus the effective dose might also be higher. Manufacturers might therefore rethink their current method of how to specify the desired image quality on CT devices.

References

Atherton J V and Huda W 1996 Energy imparted and effective doses in computed tomography *Med. Phys.* **23** 735–41

Brenner D J, Elliston C D, Hall E J and Berdon W E 2001 Estimated risks of radiation-induced fatal cancer from pediatric CT *Am. J. Roentgenol.* **176** 289–96

Brix G, Nagel H D, Stamm G, Veit R, Lechel U, Griebel J and Galanski M 2003 Radiation exposure in multi-slice versus single-slice spiral CT: results of a nationwide survey *Eur. Radiol.* **13** 1979–91

Broder J, Fordham L A and Warshauer D M 2007 Increasing utilization of computed tomography in the pediatric emergency department, 2000–2006 *Emerg. Radiol.* **14** 227–32

Chodick G, Ronckers C, Ron E and Shalev V 2006 The utilization of pediatric computed tomography in a large Isreali health maintenance organization *Pediatr. Radiol.* **36** 485–90

Committee on the Biological Effects of Ionizing Radiations (BEIR) 1980 *Health Effects of Exposure to Low Levels of Ionizing Radiation—BEIR V* (Washington, DC: The National Academic Press)

Cranley K, Gilmore B J, Fogarty G W A and Desponds L 1997 Catalogue of diagnostic x-ray spectra and other data *Report No. 78*, The Institute of Physics and Engineering in Medicine

CRCPD 2007 Nationwide evaluation of x-ray trends (NEXT)—tabulation and graphical summary of 2000 survey of computed tomography *Technical Report CRCPD Publication E-07-2* Conference of Radiation Control Program Directors, Inc. http://www.crcpd.org/Pubs/NEXT_docs/NEXT2000-CT.pdf

Cristy M and Eckerman K 1987 Specific absorbed fractions of energy at various ages from internal photon sources: I. Methods *Technical Report* ORNL/TM-8381/V1, Oak Ridge National Laboratory, TN, USA

Donnelly L F, Emery K H, Brody A S, Laor T, Gylys-Morin V M, Anton C G, Thomas S R and Frush D P 2001 Minimizing radiation dose for pediatric body applications of single-detector helical CT: strategies at a large children's hospital *Am. J. Roentgenol.* **176** 303–6

Fox S H and Toth T 2002 Dose reduction on GE CT scanners *Pediatr. Radiol.* **32** 718–23
Galanski M, Nagel H D and Stamm G 2006 Pädiatrische CT-Expositionspraxis in der Bundesrepublik Deutschland—Ergebnisse einer bundesweiten Umfrage 2005/06 *Technical Report*, Hannover, Germany: Hannover Medical School
Huda W, Atherton J V, Ware D E and Cumming W A 1997 An approach for the estimation of effective radiation dose at CT in pediatric patients *Radiology* **203** 417–22
International Atomic Energy Agency 2007 Dosimetry in diagnostic radiology: an international code of practice *Technical Reports Series No. 457* (Vienna, Austria: IAEA)
International Commission on Radiological Protection 2002 *Basic Anatomical and Physiological Data for Use in Radiological Protection: Reference Values (ICRP Publication 89)* (Oxford: Pergamon)
International Commission on Radiological Protection 2007 *Recommendations of the International Commission on Radiological Protection (ICRP Publication 103)* (Amsterdam: Elsevier)
International Commission on Radiological Protection 2009 *Adult Reference Computational Phantoms (ICRP Publication 110)* (Amsterdam: Elsevier)
Kawrakow I, Mainegra-Hing E, Rogers D W O, Tessier F and Walters B R B 2010 The EGSnrc code system: Monte Carlo simulation of electron and photon transport *PIRS Report 701* National Research Council of Canada, Ottawa, Canada, http://irs.inms.nrc.ca/software/egsnrc/documentation/pirs701.pdf
Khursheed A, Hillier M C, Shrimpton P C and Wall B F 2002 Influence of patient age on normalized effective doses calculated for CT examinations *Br. J. Radiol.* **75** 819–30
King S D and Spiers F W 1985 Photoelectron enhancement of the absorbed dose from x rays to human bone marrow: experimental and theoretical studies *Br. J. Radiol.* **58** 345–56
Kramer R 1982 Ermittlung von Konversionsfaktoren zwischen Körperdosen und relevanten Strahlungskenngrösen bei externer Röntgen- und Gamma-Bestrahlung *GSF Report S-556,* GSF—National Research Center for Environment and Health, Neuherberg, Germany
Li X, Zhang D and Liu B 2011 A practical approach to estimate the weighted CT dose index over an infinite integration length *Phys. Med. Biol.* **56** 5789–803
McCollough C H, Bruesewitz M R and Kofler J M 2006 CT dose reduction and dose management tools: overview of available options *Radiographics* **26** 503–12
Mettler F A Jr, Wiest P W, Locken J A and Kelsey C A 2000 CT scanning: patterns of use and dose *J. Radiol. Prot.* **20** 353–9
Paterson A, Frush D P and Donnelly L F 2001 Helical CT of the body: are settings adjusted for pediatric patients? *Am. J. Roentgenol.* **176** 297–301
Petoussi-Henss N, Zankl M, Fill U and Regulla D 2002 The GSF family of voxel phantoms *Phys. Med. Biol.* **47** 89–106
Poludniowski G G 2007 Calculation of x-ray spectra emerging from an x-ray tube: Part II. X-ray production and filtration in x-ray targets *Med. Phys.* **34** 2175–86
Poludniowski G, Landry G, DeBlois F, Evans P M and Verhaegen F 2009 SpekCalc: a program to calculate photon spectra from tungsten anode x-ray tubes *Phys. Med. Biol.* **54** N433–8
Rogers L F 2001 Taking care of children: check out the parameters used for helical CT *Am. J. Roentgenol.* **176** 287
Schlattl H, Zankl M and Hoeschen C 2010 Dose conversion coefficient for CT examinations of adults with automatic tube current modulation *Phys. Med. Biol.* **55** 6243–61
Schlattl H, Zankl M and Hoeschen C 2012 $CTDI_{vol}$: a suitable normalization for CT dose conversion coefficients at different tube voltages? *Proc. SPIE* **8313** 831361
Snyder W S, Ford M R, Warner G G and Fisher H L 1969 Estimates of absorbed fractions for monoenergetic photon sources uniformly distributed in various organs of a heterogeneous phantom *J. Nucl. Med.* **10** (Suppl. 3) 5–52
Stamm G and Nagel H D 2002 CT-Expo—ein neuartiges Programm zur Dosisevaluierung in der CT *Fortschr. Röntgenstr.* **174** 1570–6
Suess C and Chen X 2002 Dose optimization in pediatric CT: current technology and future innovations *Pediatr. Radiol.* **32** 729–34
Turner A C, Zankl M, DeMarco J J, Cagnon C H, Zhang D, Angel E, Cody D D, Stevens D M, McCollough C H and McNitt-Gray M F 2010 The feasibility of a scanner-independent technique to estimate organ dose from MDCT scans: using $CTDI_{vol}$ to account for differences between scanners *Med. Phys.* **37** 1816–25
Veit R, Zankl M, Petoussi N, Mannweiler E and Drexler D 1989 Tomographic anthropomorphic models: part I. Construction technique and description of models of an 8 week old baby and a 7 year old child *GSF Report 3/89* GSF—National Research Center for Environment and Health, Neuherberg, Germany
Westerman and Bryan R 2002 Radiation dose from Toshiba CT scanners *Pediatr. Radiol.* **32** 735–7
Zankl M 2010 *Handbook of Anatomical Models for Radiation Dosimetry Medical Physics and Biomedical Engineering* ed X G Xu and K F Eckerman (Boca Raton, FL: Taylor and Francis) pp 65–85

Zankl M, Panzer W and Drexler G 1993 Tomographic anthropomorphic models: part II. Organ doses from computed tomographic examinations in paediatric radiology *GSF Report 30/93* GSF—National Research Center for Environment and Health, Neuherberg, Germany

Zankl M, Veit R, Williams G, Schneider K, Fendel H, Petoussi N and Drexler G 1988 The construction of computer tomographic phantoms and their application in radiology and radiation protection *Radiat. Environ. Biophys.* **27** 153–64

Zhang D, Zankl M, DeMarco J J, Cagnon C H, Angel E, Turner A C and McNitt-Gray M F 2009 Reducing radiation dose to selected organs by selecting the tube start angle in MDCT helical scans: a Monte Carlo based study *Med. Phys.* **36** 5654–64